Quark spin-orbit correlations in spin-0 and spin-1 mesons using the light-front quark model

Ritwik Acharyya,[*] Satyajit Puhan,[†] and Harleen Dahiya[‡]

Department of Physics, Dr. B. R. Ambedkar National Institute of Technology, Jalandhar 144008, India

(Received 25 June 2024; accepted 15 July 2024; published 14 August 2024)

We investigate the spin-orbital angular momentum correlations for the active quark inside the light and heavy mesons for both the spin-0 and spin-1 cases. These correlations can be derived from the generalized transverse-momentum-dependent distributions as well as the generalized parton distributions. We employ the overlap representation of light-front wave functions in the light-front quark model to calculate our analytical results. The dependence of spin-orbit correlations (SOCs) on the longitudinal momentum fraction x as well as the transverse-momentum-dependence $\mathbf{k}_\perp$ is graphically presented. Even though the SOCs have already been studied for the spin-0 pions and kaons in other approaches, no calculations for the other light and heavy spin-0 mesons have been reported in the literature. Further, the correlations for any of the light and heavy spin-1 mesons are studied for the first time in the present work.

DOI: 10.1103/PhysRevD.110.034020

I. INTRODUCTION

Quantum chromodynamics (QCD) [1–3] describes the production of hadrons by incorporating strong interactions among quarks, antiquarks, and gluons. One of the most significant problems and an avenue for improving our comprehension of QCD and confinement is to decipher the multidimensional structure of a hadron, thus providing insight into several nonperturbative aspects of QCD. Hadrons possess partons inside them, and the respective partonic states can be described by six-dimensional phase-space distributions called Wigner distributions [4,5]. Wigner distributions are the quantum-mechanical constructions that are closest to a classical probability density in phase space. The probability density of discovering a parton (gluon or quark) carrying the parent hadron's light-front (LF) longitudinal momentum fraction x is described by the parton distribution function (PDF) [4–11]. For the description of observables that are also sensitive to the transverse kinematics of a parton, the concept of PDFs has been extended to transverse-momentum-dependent parton distributions (TMDs) [12–19] and generalized parton distributions (GPDs) [20–27] to include the information of transverse momentum and transverse coordinate distributions, respectively. After a few phase-space reductions, Wigner distributions reduce to TMDs and GPDs. Both TMDs and GPDs present a three-dimensional visualization of the hadron. The Wigner distributions integrated over the transverse momenta reduce to the GPDs at zero skewness ($\zeta = 0$) [28]. On the other hand, integrating it over the transverse impact parameter, with zero momentum transfer, they reduce to the TMDs. TMDs can be measured in certain reactions like semi-inclusive deep inelastic scattering [29,30], Drell-Yan processes [16,31–34], and $Z^0/W^\pm$ production [35–37]. GPDs are extracted from the QCD description of hard exclusive reactions like deeply virtual Compton scattering [21,38–41] and deeply virtual meson production [42,43]. Analyzing the GPDs can reveal details about the quarks' spatial distributions. Further, Wigner distributions are Fourier transforms of the generalized transverse-momentum-dependent distributions (GTMDs) [44,45] from the transverse momentum transfer $\Delta_\perp$ to the impact parameter $b_\perp$, without integration over the LF energy. GTMDs are functions of the LF three momentum of the parton as well as the momentum transfer to the hadron [28].

The spin-orbit correlations (SOCs) between a hadron and a quark can be explained on the basis of the phase-space average of Wigner distributions. Comprehending spin composition of hadrons has been a fascinating subject of research lately [46–49], and understanding the multidimensional structure makes it possible to analyze characteristics such as SOCs, spin-spin correlations, quark-gluon correlations, and other such interactions. It would be interesting to explore the connection of the GPDs and GTMDs of spin-0 and spin-1 mesons with their spin-orbital angular momentum correlations and proceed to calculate their analytical results. In particular, the correlations

[*]Contact author: ritwikacharyya2001@gmail.com
[†]Contact author: puhansatyajit@gmail.com
[‡]Contact author: dahiyah@nitj.ac.in

between the hadron spin and the orbital motion of partons inside the hadron can bring much bigger insight into the spin structure of the hadrons [50]. Given that a parton's orbital angular momentum (OAM) and spin contributions have intrinsic negative parity, the only nonvanishing single-parton ($a = q, G$) correlations allowed by parity invariance are $\mathbf{S}_a \cdot \mathbf{S}_N$, $\mathbf{L}_a \cdot \mathbf{S}_N$, and $\mathbf{S}_a \cdot \mathbf{L}_a$. Here, $\mathbf{L}_{q,G}$ represents the quark (or gluon) OAM, $\mathbf{S}_N$ is the spin of the hadron, and $\mathbf{S}_{q,G}$ portrays the spin of the constituent quark (or gluon) [50]. The initial two types of correlations are commonly referred to as OAM and spin contributions of parton a to the spin of the hadron, whereas the third and final type is the parton's SOC. We use the difference between the right-handed and left-handed contributions of the quark longitudinal OAM to describe the quark longitudinal SOC, which is expressed by C_z^q.

Dirac, in 1949 [51], recognized that one may set up a dynamical theory in which the dynamical variables refer to the physical conditions on a front $x^+ = 0$. The resulting dynamics is called the LF dynamics, which Dirac referred to as "front-form" for brevity. The LF dynamics [30,52–54] is a beneficial model framework, which helps us study the internal structure of hadrons [30,51] and has direct applications in the Minkowski space [55]. LF quantization provides a framework to describe the perturbative and nonperturbative regimes of QCD. LF dynamics can be realized by a number of different models, and for this work we have adopted the LF quark model (LFQM) [56–58]. The LFQM is based on the algebra of generators of the Lorentz group in the LF dynamics [59]. The component quark and antiquark in a bound state must be on-mass shell in conventional LFQM [2,60–62]. The spin-orbit wave function is derived from the conventional time-independent spin-orbit wave function supplied by the quantum numbers J^{PC} [63] using the well-known Melosh transformation, which is independent of interactions [64]. The LFQM is primarily concerned with the valence quarks of hadrons, which are among the primary elements responsible for the overall composition and properties of hadrons. With accurate parameter choices, the model describes several hadron characteristics, including form factors (FFs), distribution amplitudes, decay constants, etc., thus establishing a phenomenological link between hadron properties and the wave function of the quark constituents, which has been successful in many instances.

Quark SOCs have been studied earlier for the spin-$\frac{1}{2}$ hadrons [65] and also investigated for the case of spin-0 hadrons like pions and kaons [50,66]. However, no work has been reported for the remaining members of the spin-0 mesons. Further, the spin-1 mesons (light and heavy) have also remained unexplored in this regard. We may obtain special insights into the orbital motion of quarks and their intrinsic longitudinal spin inside spin-0 and spin-1 mesons, owing to the quark SOC [50]. In light of the successes of the LFQM and the importance of the quark SOCs, it becomes essential to extend this work across all members in both the spin-0 and spin-1 meson spectrum. To make the application of this work broader, we have included the light as well as heavy mesons for both the spin-0 and spin-1 cases. We have utilized the conventional definition of the leading-twist GTMD $G_{1,1}$ in our calculations and have solved the correlators for the leading-twist GPD case. To derive the outcome for the SOC, we have integrated the GTMD $G_{1,1}$ twice in terms of transverse momentum $\mathbf{k}_\perp$ and fraction of momentum transfer to the active quark x involving the entire wave function of the LFQM. We have visualized the behavior of the spin-orbit correlator C_z^q in our chosen model via two-dimensional plots with respect to the longitudinal momentum fraction x and transverse momenta of quark $\mathbf{k}_\perp$. We have also presented the model-dependent results for the pion and kaon. Further, the physical implications of the SOC for both the spin-0 and spin-1 light and heavy mesons have been discussed.

This paper is arranged as follows. In Sec. II, we have presented the correlation between the quark spin and OAM inside the hadron. In Sec. III, we have quantitatively discussed LFQM: the model employed to define our LF wave functions (LFWFs). In Sec. IV, we have shown how the spin-OAM correlations can be methodically derived from the GPDs and the GTMDs. These relations have been presented for both the light and heavy spin-0 and spin-1 mesons. Further, in Sec. V, we have defined our model parameters and presented our model results for the SOC. Finally, we have summarized our results in Sec. VI.

II. SPIN-ORBIT CORRELATION

The local gauge-invariant LF operators for the quark longitudinal spin and OAM have been of unique interest since they enter Ji's decomposition of the total angular momentum operator in QCD [46,50], which is given as

$$\hat{J}_z = \hat{S}_z^q + \hat{L}_z^q + \hat{J}_z^G. \tag{1}$$

Here, $\hat{L}_z^q$ refers to the gauge-invariant LF quark longitudinal OAM, which can be further decomposed into right-handed and left-handed quark contributions as

$$\hat{L}_z^q = \int d^3x \frac{1}{2} \bar{\psi}\gamma^+ (\mathbf{x} \times i\overleftrightarrow{\mathbf{D}})_z \psi = \hat{L}_z^{qR} + \hat{L}_z^{qL}, \tag{2}$$

where the symmetric covariant derivative is defined by $\overleftrightarrow{\mathbf{D}} = \overleftarrow{\partial} - \overrightarrow{\partial} - 2ig\mathbf{A}$ [50]. $\psi_{R,L} = \frac{1}{2}(\mathbf{I} \pm \gamma_5)\psi$ and $d^3x = dx^- d^2x_\perp$. The knowledge and understanding of quark SOCs give us a complete characterization of the hadron's internal structure. The local gauge-invariant correlation is described by

$$\hat{C}_z^q = \int d^3x \frac{1}{2} \overline{\psi}\gamma^+\gamma_5 (\mathbf{x} \times i\overleftrightarrow{\mathbf{D}})_z \psi = \hat{L}_z^{qR} - \hat{L}_z^{qL}. \tag{3}$$

The quark OAM operator may be represented in terms of the gauge-invariant energy-momentum tensor as follows [65]:

$$\hat{L}_z^q = \int d^3x \left(x^1 \hat{T_q^{+2}} - x^2 \hat{T_q^{+1}} \right), \tag{4}$$

where $T^{\hat{\mu}\nu}$ is the energy-momentum tensor operator given by

$$T_q^{\hat{\mu}\nu} = \frac{1}{2}\overline{\psi}\gamma^\mu i\overleftrightarrow{\mathbf{D}}^\nu \psi \tag{5}$$

$$= T_{qR}^{\hat{\mu}\nu} - T_{qL}^{\hat{\mu}\nu} Fq, \tag{6}$$

and $T_{R,L}^{\hat{\mu}\nu} = \frac{1}{2}\overline{\psi}_{R,L}\gamma^\mu i\overleftrightarrow{\mathbf{D}}^\nu \psi_{R,L}$. Further, the quark SOC operator is given as follows:

$$\hat{C}_z^q = \int d^3x \left(x^1 \hat{T_{q5}^{+2}} - x^2 \hat{T_{q5}^{+1}} \right), \tag{7}$$

where $T_{q5}^{\hat{\mu}\nu}$ may be regarded as the parity-odd partner of $T^{\hat{\mu}\nu}$ and can be expressed as [65]

$$T_{q5}^{\hat{\mu}\nu} = \frac{1}{2}\overline{\psi}\gamma^\mu\gamma_5 i\overleftrightarrow{\mathbf{D}}^\nu \psi \tag{8}$$

$$= T_{qR}^{\hat{\mu}\nu} + T_{qL}^{\hat{\mu}\nu}. \tag{9}$$

The nonforward matrix components of $T_{q5}^{\hat{\mu}\nu}$ inserted between two meson states may be parametrized as a sum of two form factors $\tilde{\mathcal{C}}_q(t)$ and $\tilde{\mathcal{F}}_q(t)$ [67–70], which can be expressed as

$$\langle k'|T_{q5}^{\hat{\mu}\nu}(0)|k\rangle = -\frac{P^{[\mu_{i\epsilon}\nu]+\Delta P}}{2P^+}(\tilde{\mathcal{C}}_q(t) - 2\tilde{\mathcal{F}}_q(t)) + i\epsilon^{\mu\nu\Delta P}\tilde{\mathcal{F}}_q(t) + \mathcal{O}(\Delta^2). \tag{10}$$

Substituting Eq. (10) into the matrix elements of Eq. (7), within the symmetric LF frame ($\mathbf{P}_\perp = \mathbf{0}_\perp$), we get

$$C_z^q = \frac{\langle p|\hat{C}_z^q|p\rangle}{\langle p|p\rangle} = \tilde{\mathcal{C}}_q(0). \tag{11}$$

Thus, we just need to compute the form factor $\tilde{\mathcal{C}}_q(t)$ in order to determine the quark SOCs for the mesons.

III. LIGHT-FRONT QUARK MODEL

In the LF technique, a sequence of LFWFs in the Fock-state basis are used to define the wave functions of the meson describing a composite state at a certain LF time [71]. The meson eigenstate $|\mathbb{M}(P^+, \mathbf{P}_\perp, S_z)\rangle$ can be expressed in terms of its component eigenstate $|n\rangle$ using the LF Fock-state expansion and can be expressed as [28,66,72]

$$|\mathbb{M}(P^+, \mathbf{P}_\perp, S_z)\rangle = \sum_{n,\lambda_i}\int \prod_{i=1}^{n}\frac{dx_i d^2\mathbf{k}_{\perp i}}{\sqrt{x_i}16\pi^3} 16\pi^3\delta\left(1-\sum_{i=1}^{n}x^i\right)\delta^{(2)}\left(\sum_{i=1}^{n}\mathbf{k}_{\perp i}\right)|n; x_iP^+, x_i\mathbf{P}_\perp + \mathbf{k}_{\perp i}, \lambda_i\rangle\Psi^\Lambda_{\lambda_1,\lambda_2}(x_i, \mathbf{k}_{\perp i}). \tag{12}$$

Here, we denote $P = (P^+, P^-, P_\perp)$ as the meson's total momentum and S_z as the longitudinal spin projection of the target. The LF momentum coordinates and relative momentum fractions of the mesonic components are denoted by $\mathbf{k}_{\perp i}$ and $x_i = k_i^+/P^+$, respectively. The quark's transverse and longitudinal momentum fractions are represented by the symbols $\mathbf{k}_\perp$ and x, respectively. In contrast, $1-x$ and $-\mathbf{k}_\perp$, respectively, describe the same for the antiquark spectator. λ_i is the helicity, and m_i is the mass of the ith constituent correspondingly. In Eq. (12), $x_i\mathbf{P}_\perp + \mathbf{k}_{\perp i} = \mathbf{p}_{\perp i}$ is the physical transverse momentum. $\Psi^\Lambda_{\lambda_1,\lambda_2}(x_i, \mathbf{k}_{\perp i})$ is the LFWF with different spin and helicity projections, and $\lambda_{1(2)}$ describes the helicity of the quark (antiquark) in the meson. Also, $\Lambda = T$ refers to the transverse spin projections of the mesons. To simplify our calculations, we have considered the minimal Fock-state description of the meson in the form of a quark-antiquark pair and is expressed as [73]

$$|\mathbb{M}(P,S)\rangle = \sum_{\lambda_1,\lambda_2}\int \frac{dxd^2\mathbf{k}_\perp}{16\pi^3\sqrt{x(1-x)}}|x,\mathbf{k}_\perp,\lambda_1,\lambda_2\rangle\Psi^\Lambda_{\lambda_1,\lambda_2}(x,\mathbf{k}_\perp). \tag{13}$$

The momenta of the meson (P), constituent quark (k_1), and antiquark (k_2) in the LFQM are given as

$$P = \left(P^+, \frac{M^2}{P^+}, \mathbf{0}_\perp\right), \tag{14}$$

$$k_1 = \left(xP^+, \frac{\mathbf{k}_\perp^2 + m_q^2}{xP^+}, \mathbf{k}_\perp\right), \tag{15}$$

$$k_2 = \left((1-x)P^+, \frac{\mathbf{k}_\perp^2 + m_{\bar{q}}^2}{(1-x)P^+}, -\mathbf{k}_\perp\right). \tag{16}$$

Here, $m_q(m_{\bar{q}})$ refers to the boost invariant mass of the quark (antiquark), and M refers to the mass of the meson, which is given by

$$M^2 = \frac{\mathbf{k}_\perp^2 + m_q^2}{x} + \frac{\mathbf{k}_\perp^2 + m_{\bar{q}}^2}{1-x}. \tag{17}$$

The LF meson wave function is expressed as [74,75]

$$\Psi^\Lambda_{\lambda_1,\lambda_2}(x,\mathbf{k}_\perp) = \phi(x,\mathbf{k}_\perp)X^\Lambda_{\lambda_1,\lambda_2}(x,\mathbf{k}_\perp). \tag{18}$$

Here, $X^{\Lambda}_{\lambda_1,\lambda_2}(x,\mathbf{k}_\perp)$ represents the spin wave function, and $\phi(x,\mathbf{k}_\perp)$ is the momentum-space wave function of the meson, respectively. Let us begin our discussions with spin-0 meson. The spin wave functions are derived through the Melosh-Wigner rotation [76–78], and for spin-0 mesons, they are expressed as [79]

$$X^{\mathcal{SP}0}(x,\mathbf{k}_\perp)=\sum_{\lambda_1,\lambda_2}K_0(x,\mathbf{k}_\perp,\lambda_1,\lambda_2)X_1^{\lambda_1}X_2^{\lambda_2}, \tag{19}$$

where $\mathcal{SP}0$ stands for the spin-0 meson. $K_0(x,\mathbf{k}_\perp,\lambda_1,\lambda_2)$ is the coefficient of the spin wave function. The different helicity combinations are described as

$$K_0(x,\mathbf{k}_\perp,\uparrow,\downarrow)=[(xM+m_q)((1-x)M+m_{\bar{q}})-k_\perp^2]/\sqrt{2}w_1w_2, \tag{20}$$

$$K_0(x,\mathbf{k}_\perp,\downarrow,\uparrow)=-[(xM+m_q)((1-x)M+m_{\bar{q}})-k_\perp^2]/\sqrt{2}w_1w_2, \tag{21}$$

$$K_0(x,\mathbf{k}_\perp,\uparrow,\uparrow)=[(xM+m_q)k_2^L-((1-x)M+m_{\bar{q}})k_1^L]/\sqrt{2}w_1w_2, \tag{22}$$

$$K_0(x,\mathbf{k}_\perp,\downarrow,\downarrow)=[(xM+m_q)k_2^R-((1-x)M+m_{\bar{q}})k_1^R]/\sqrt{2}w_1w_2. \tag{23}$$

Here, the subscripts $\uparrow$ and $\downarrow$ denote the transverse polarizations of the quark along the directions $\hat{e}_x$ and $-\hat{e}_x$, respectively, and

$$w_1=[(xM+m_q)^2+\mathbf{k}_\perp^2]^{\frac{1}{2}}, \tag{24}$$

$$w_2=[((1-x)M+m_{\bar{q}})^2+\mathbf{k}_\perp^2]^{\frac{1}{2}}. \tag{25}$$

For the spin-1 mesons, the spin wave functions occurring in Eq. (18) take the form for $\Lambda=T(+)$ as [80]

$$X^{T(+)}_{+,+}(x,\mathbf{k}_\perp)=\frac{m_q(M+2m)+\mathbf{k}_\perp^2}{(M+m_q)\sqrt{m_q^2+\mathbf{k}_\perp^2}}, \tag{26}$$

$$X^{T(+)}_{-,+}(x,\mathbf{k}_\perp)=-\frac{k_R((1-x)M+m_q)}{(M+m_q)\sqrt{m_q^2+\mathbf{k}_\perp^2}}, \tag{27}$$

$$X^{T(+)}_{+,-}(x,\mathbf{k}_\perp)=\frac{k_R(xM+m_q)}{(M+m_q)\sqrt{m_q^2+\mathbf{k}_\perp^2}}, \tag{28}$$

$$X^{T(+)}_{-,-}(x,\mathbf{k}_\perp)=-\frac{k_R^2}{(M+m_q)\sqrt{m_q^2+\mathbf{k}_\perp^2}}. \tag{29}$$

Similarly, the spin wave functions occurring in Eq. (18) take the form for $\Lambda=T(-)$ as

$$X^{T(-)}_{+,+}(x,\mathbf{k}_\perp)=-\frac{k_L^2}{(m_q+M)\sqrt{m_q^2+\mathbf{k}_\perp^2}}, \tag{30}$$

$$X^{T(-)}_{-,+}(x,\mathbf{k}_\perp)=-\frac{(xM+m_q)k_L}{(M+m_q)\sqrt{m_q^2+\mathbf{k}_\perp^2}}, \tag{31}$$

$$X^{T(-)}_{+,-}(x,\mathbf{k}_\perp)=\frac{((1-x)M+m_q)k_L}{(M+m_q)\sqrt{m_q^2+\mathbf{k}_\perp^2}}, \tag{32}$$

$$X^{T(-)}_{-,-}(x,\mathbf{k}_\perp)=\frac{m_q(M+2m)+\mathbf{k}_\perp^2}{(M+m_q)\sqrt{m_q^2+\mathbf{k}_\perp^2}}, \tag{33}$$

where

$$k_{R(L)}=k_x\pm ik_y.$$

The momentum-space wave function can be described using the Brodsky-Huang-Lepage method as [81]

$$\phi(x,\mathbf{k}_\perp)=A\exp\left[-\frac{\frac{m_q^2+\mathbf{k}_\perp^2}{x}+\frac{m_{\bar{q}}^2+\mathbf{k}_\perp^2}{1-x}}{8\beta^2}-\frac{(m_q^2-m_{\bar{q}}^2)^2}{8\beta^2\left(\frac{m_q^2+\mathbf{k}_\perp^2}{x}+\frac{m_{\bar{q}}^2+\mathbf{k}_\perp^2}{1-x}\right)}\right]. \tag{34}$$

Here, β refers to the harmonic oscillator (HO) scale parameter and A to the normalization constant. For $m_q=m_{\bar{q}}=m$, we have pionlike mesons, and for $m_q\neq m_{\bar{q}}$, we have kaonlike mesons.

IV. CONNECTING SOC TO GPDS AND GTMDS

The energy-momentum tensor operator $T^{\hat{\mu}\nu}$ has no fundamental probe that can couple to its parity-odd partner $T^{\hat{\mu}\nu}_{q5}$ in high energy physics. However, by connecting the respective form FFs to the exact moments of the GTMDs or

GPDs, we can obtain a representation of $T^{\hat{\mu}\nu}_{q5}$ [50]. The relationship between the FFs may be derived employing the following QCD relation:

$$\overline{\phi}\gamma^{[\mu}\gamma_5 i\overleftrightarrow{\mathbf{D}}^{\nu]}\phi = 2m\bar{\phi}i\sigma^{\mu\nu}\gamma_5\phi - \epsilon^{\mu\nu\alpha\beta}\partial_\alpha(\bar{\psi}\gamma_\beta\phi). \tag{35}$$

A. GPD approach

When we focus on the matrix's off-diagonal components in Eq. (35), the left-hand side represents the SOC [50], whereas the right-hand side parametrizes the vector and tensor local correlators as [65]

$$\langle p'|\bar{\phi}\gamma^\mu\phi|p\rangle = \Gamma^\mu_{qV}, \tag{36}$$

$$\langle p'|\bar{\phi}i\sigma^{\mu\nu}\gamma_5\phi|p\rangle = \Gamma^{\mu\nu}_{qT}, \tag{37}$$

where

$$\Gamma^{\mu\nu}_{qT} = \frac{2i\epsilon^{\mu\nu\alpha\beta}\Delta_\alpha P_\beta}{M}\int H^q_1(x,\zeta,t)dx, \tag{38}$$

$$\Gamma^{\mu}_{qV} = 2P^\mu\int F^q_1(x,\zeta,t)dx. \tag{39}$$

Here, $\zeta = -\Delta^+/2P^+$ is the skewness variable with Δ being the momentum transfer. The functions $H^q_1(x,\zeta,t) = H_1$ (for simplicity) and $F^q_1(x,\zeta,t) = F_1$ (for simplicity) are defined as GPDs [82,83] of the meson. $H^q_1(x,\zeta,t)$ represents the axial-vector LF quark correlator, and $F^q_1(x,\zeta,t)$ represents the tensor LF quark correlator. They are given as

$$\frac{1}{2}\int\frac{dy^-}{2\pi}e^{ixP^+y^-}\langle p'|\bar{\phi}\left(-\frac{y^-}{2}\right)i\sigma^{j+}\gamma_5\phi\left(\frac{y^-}{2}\right)|p\rangle = -\frac{i\epsilon^{ij}_\perp\Delta^i_\perp}{M}H^q_1(x,\zeta,t), \tag{40}$$

$$\frac{1}{2}\int\frac{dy^-}{2\pi}e^{ixP^+y^-}\langle p'|\bar{\phi}\left(-\frac{y^-}{2}\right)\gamma^+\phi\left(\frac{y^-}{2}\right)|p\rangle = F^q_1(x,\zeta,t). \tag{41}$$

Hence, the SOC may be ascertained through the combinations of the moments of $F^q_1(x,\zeta,t)$ and $H^q_1(x,\zeta,t)$,

$$\tilde{C}_q(t) = \int dx\left(\frac{m_q}{M}H^q_1(x,\zeta,t) - \frac{1}{2}F^q_1(x,\zeta,t)\right). \tag{42}$$

Therefore, the expectation value of the SOC can be expressed analytically in the form of GPDs as

$$C^q_z = \int dx\left(\frac{m_q}{M}H^q_1(x,0,0) - \frac{1}{2}F^q_1(x,0,0)\right). \tag{43}$$

B. GTMD approach

The SOC can also be expressed in the form of GTMDs [5,28,66]. We can exhibit C^q_z in the form of one of the leading-twist-2 GTMDs $G_{1,1}(x,\zeta,\mathbf{k}^2_\perp,\mathbf{k}_\perp\cdot\mathbf{\Delta}_\perp,\mathbf{\Delta}^2_\perp) = G_{1,1}$ (for simplicity) that are related to unpolarized meson states. For the present work, we consider the case of zero skewness, i.e., $\zeta = 0$. We have

$$C^q_z = \int dx d^2\mathbf{k}_\perp\frac{\mathbf{k}^2_\perp}{M^2}G_{1,1}(x,0,\mathbf{k}^2_\perp,0,0). \tag{44}$$

We consider here the TMD limit, i.e., $\Delta = 0$, which reduces the GTMD to a function of only x and $\mathbf{k}_\perp$. The GTMDs are connected to the Wigner correlator as follows [66]:

$$\hat{W}^{[\gamma^+]} = F_{1,1}, \tag{45}$$

$$\hat{W}^{[\gamma^+\gamma_5]} = -\frac{i\epsilon^{ij}_\perp\mathbf{k}^i_\perp\Delta^i_\perp}{M^2}G_{1,1}, \tag{46}$$

$$\hat{W}^{[i\sigma^{j+}\gamma_5]} = -\frac{i\epsilon^{ij}_\perp\mathbf{k}^i_\perp}{M^2}H_{1,1} - \frac{i\epsilon^{ij}_\perp\Delta^i_\perp}{M^2}H_{1,2}. \tag{47}$$

Here, $\epsilon^{ij}_\perp = \epsilon^{-+ij}$ is the antisymmetric tensor, $\epsilon^{0123} = 1$ and $\sigma^{ab} = \frac{i}{2}[\gamma^a,\gamma^b]$. The Wigner correlator is denoted by the symbol $W^{[\Gamma]}$ and can be expressed as

$$\mathrm{W}^{[\Gamma]}(x,P,\Delta,\mathbf{k}_\perp) = \frac{1}{2}\mathrm{Tr}[W(x,P,\Delta,\mathbf{k}_\perp)\Gamma] \tag{48}$$

$$= \frac{1}{2}\int\frac{dz^-d^2z_\perp}{2(2\pi)^3}e^{ik.z}\langle p'|\bar{\psi}\left(-\frac{z^-}{2}\right)\times\Gamma\mathcal{W}\psi\left(\frac{z^-}{2}\right)|p\rangle|_{z^+=0}. \tag{49}$$

Here, $W^{[\Gamma]}(x,P,\Delta,\mathbf{k}_\perp)$ is the generalized parton correlation function (GPCF) of the meson. $\mathcal{W}$ refers to the Wilson lines, which result from the parallel transit of gauge variables across closed loops. To simplify our present calculations, we consider $\mathcal{W}$ to be equal to 1. Γ is the operator sandwiched between the initial and final meson states (p and p'), respectively. The GTMDs can be obtained from the GPCFs by integrating over the quark momentum $\mathbf{k}_\perp$ [84]. F_1 and H_1 are the GPD limits of the more general GTMDs $F_{1,1}$ and $G_{1,1}$. However, the GTMD $G_{1,1}$ does not have an equivalent GPD due to its $\mathbf{k}_\perp$-odd property [50]. Therefore, the relation stated in Eq. (44) provides an alternative formulation for the SOC based on a broader parton correlation structure. In the overlap representation, the leading-twist generalized correlator for GTMDs can be expressed as [71,85]

$$W^{[\gamma^+]} = \frac{1}{16\pi^3}\sum_{\lambda_{\bar{q}}}\Big(\phi^*_{\downarrow\lambda_{\bar{q}}}(x'',\mathbf{k}''_\perp)\phi_{\downarrow\lambda_{\bar{q}}}(x',\mathbf{k}'_\perp) + \phi^*_{\uparrow\lambda_{\bar{q}}}(x'',\mathbf{k}''_\perp)\phi_{\uparrow\lambda_{\bar{q}}}(x',\mathbf{k}'_\perp)\Big), \tag{50}$$

$$W^{[\gamma^+\gamma_5]} = \frac{1}{16\pi^3}\sum_{\lambda_{\bar{q}}}\Big(\phi^*_{\uparrow\lambda_{\bar{q}}}(x'',\mathbf{k}''_\perp)\phi_{\uparrow\lambda_{\bar{q}}}(x',\mathbf{k}'_\perp) - \phi^*_{\downarrow\lambda_{\bar{q}}}(x'',\mathbf{k}''_\perp)\phi_{\downarrow\lambda_{\bar{q}}}(x',\mathbf{k}'_\perp)\Big), \tag{51}$$

$$W^{[i\sigma^{j+}\gamma_5]} = \frac{1}{16\pi^3}\sum_{\lambda_{\bar{q}}}\Big(\phi^*_{\uparrow\lambda_{\bar{q}}}(x'',\mathbf{k}''_\perp)\phi_{\uparrow\lambda_{\bar{q}}}(x',\mathbf{k}'_\perp) - \phi^*_{\downarrow\lambda_{\bar{q}}}(x'',\mathbf{k}''_\perp)\phi_{\downarrow\lambda_{\bar{q}}}(x',\mathbf{k}'_\perp)\Big). \tag{52}$$

The arguments of the initial-state wave functions in Eqs. (50)–(52) are given as

$$x_1 = \frac{x-\zeta/2}{1-\zeta/2},$$
$$k_{\perp 1} = k_\perp - \frac{1-x}{1-\zeta/2}\frac{\Delta_\perp}{2},$$

and for the final-state wave functions, they are given as

$$x_2 = \frac{x+\zeta/2}{1+\zeta/2},$$
$$k_{\perp 2} = k_\perp + \frac{1-x}{1+\zeta/2}\frac{\Delta_\perp}{2}.$$

C. Spin-0 mesons

The leading-twist GTMDs that we mention in this work are $F_{1,1}$, $G_{1,1}$, $H_{1,1}$, and $H_{1,2}$. Using the LFWFs of the form of Eq. (34), along with the overlap representation for $W^{[\Gamma]}$, we obtain the explicit expressions for the GTMDs of mesons having disparate quark and antiquark masses [66]

$$F_{1,1} = \frac{1}{16\pi^3}[\mathbf{k}_\perp^2 + \mathcal{M}_2\mathcal{M}_1]\times\frac{\phi(x_1,\mathbf{k}_{\perp 1})\phi^\dagger(x_2,\mathbf{k}_{\perp 2})}{\sqrt{j_2^2+\mathbf{k}_{\perp 2}^2}\sqrt{j_1^2+\mathbf{k}_{\perp 1}^2}}, \tag{53}$$

$$G_{1,1} = -\frac{M^2}{16\pi^3}\frac{(2-x_2-x_1)}{2}\frac{\phi(x_1,\mathbf{k}_{\perp 1})\phi^\dagger(x_2,\mathbf{k}_{\perp 2})}{\sqrt{j_2^2+\mathbf{k}_{\perp 2}^2}\sqrt{j_1^2+\mathbf{k}_{\perp 1}^2}}, \tag{54}$$

$$H_{1,1} = -\frac{M}{16\pi^3}[\mathcal{M}_1-\mathcal{M}_2]\frac{\phi(x_1,\mathbf{k}_{\perp 1})\phi^\dagger(x_2,\mathbf{k}_{\perp 2})}{\sqrt{j_2^2+\mathbf{k}_{\perp 2}^2}\sqrt{j_1^2+\mathbf{k}_{\perp 1}^2}}, \tag{55}$$

$$H_{1,2} = \frac{M}{16\pi^3}\left[\mathcal{M}_1\frac{(1-x_2)}{2} - \mathcal{M}_2\frac{(1-x_1)}{2}\right]\times\frac{\phi(x_1,\mathbf{k}_{\perp 1})\phi^\dagger(x_2,\mathbf{k}_{\perp 2})}{\sqrt{j_2^2+\mathbf{k}_{\perp 2}^2}\sqrt{j_1^2+\mathbf{k}_{\perp 1}^2}}, \tag{56}$$

where

$$\mathcal{M}_1 = \frac{1-x}{1+\zeta}m_q + \frac{x+\zeta}{1+\zeta}m_{\bar{q}}, \tag{57}$$

$$\mathcal{M}_2 = \frac{1-x}{1-\zeta}m_q + \frac{x-\zeta}{1-\zeta}m_{\bar{q}}, \tag{58}$$

$$j_1^2 = \frac{1-x}{1+\zeta}m_q^2 + \frac{x+\zeta}{1+\zeta}m_{\bar{q}}^2 - \frac{(1-x)(x+\zeta)}{(1+\zeta^2)^2}(m_q-m_{\bar{q}})^2, \tag{59}$$

$$j_2^2 = \frac{1-x}{1-\zeta}m_q^2 + \frac{x-\zeta}{1-\zeta}m_{\bar{q}}^2 - \frac{(1-x)(x-\zeta)}{(1-\zeta^2)^2}(m_q-m_{\bar{q}})^2. \tag{60}$$

In this section, we have presented the quark GTMDs of mesons with respect to the longitudinal momentum fraction carried by quark x. Being the mother distributions, GTMDs have the versatility to be reduced to the corresponding GPDs and TMDs. The $\mathbf{k}_\perp$-even GTMDs are reduced to the respective GPDs after integrating over $\mathbf{k}_\perp$ [50]. We have

$$F_1^q(x,\zeta,t) = \int d^2\mathbf{k}_\perp F_{1,1}, \tag{61}$$

$$H_1^q(x,\zeta,t) = \int d^2\mathbf{k}_\perp\left(\frac{\mathbf{k}_\perp.\Delta_\perp}{\Delta_\perp^2}H_{1,1} + H_{1,2}\right). \tag{62}$$

Further, the antiquark GTMDs are related to the quark GTMDs by the relation

$$F^u(x,\mathbf{k}_\perp^2,\zeta,\Delta_\perp^2,\mathbf{k}_\perp.\Delta_\perp,m_q,m_{\bar{q}}) = F^{\bar{s}}(1-x,\mathbf{k}_\perp^2,\zeta,\Delta_\perp^2,-\mathbf{k}_\perp.\Delta_\perp,m_{\bar{q}},m_q). \tag{63}$$

D. Spin-1 mesons

For spin-1 mesons, our spatial wave function will remain the same, but there will be an addition of a spin wave part. Since we are essentially dealing with TMDs, in this section we define the explicit expression of $g_1(x,\mathbf{k}_\perp^2)$ T-even TMDs [12,80] in the LFQM using the wave functions in Eq. (34). We have

$$g_1(x,\mathbf{k}_\perp^2) = \frac{M}{2(2\pi)^3}(2m_q + M)[(2\mathbf{k}_\perp^2 + m_q(M+2m_q)) + m_q M(1-2x)] \tag{64}$$

$$\times \frac{|\psi(x,\mathbf{k}_\perp^2)|^2}{\omega^2}, \tag{65}$$

where

$$\omega = (M+2m_q)\sqrt{\mathbf{k}_\perp^2 + m_q^2}. \tag{66}$$

V. NUMERICAL RESULTS

For the numerical calculations, we have taken the input parameters of the LFQM for different quark masses (m_q, m_b, m_c, m_s) with $q = (u,d)$ and different variational HO parameters $(\beta_{q\bar{q}},\beta_{q\bar{c}},\beta_{q\bar{b}},\beta_{q\bar{s}},\beta_{s\bar{c}},\beta_{b\bar{b}},\beta_{c\bar{c}},\beta_{s\bar{b}},\beta_{c\bar{b}})$ from Refs. [2,50]. These parameters have been presented in Table I and obtained by reproducing the mass spectra using the variational principle, which has been successful in computing various physical properties such as decay constants, electromagnetic form factors, and distribution amplitudes [2].

In order to compute the spin-orbit correlators using the $G_{1,1}$ GTMD for the respective meson, we have used Eq. (44) along with the quark masses and HO parameters from Table I. We have summarized the calculated results of the SOC inside various spin-0 mesons in Table II. From the table, we observe that the sign of the correlation is negative for all spin-0 mesons, which clearly implies that the quark longitudinal spin and quark OAM tend to be antialigned inside the respective spin-0 meson. This correlation between the quark spin and OAM takes into account the effective number of quarks inside a parent hadron [5]. Therefore, it would be interesting to compare the absolute value of the spin-0 mesons to that of the nucleons. It is clear from the results that the magnitude of SOC for the mesons is less than that of the nucleon ($C_z^{u/n} = -0.9$ and $C_z^{d/n} = -0.53$ [65]) pointing toward a weaker correlation inside the mesons, which seems to be due to more effective quarks inside the nucleons in comparison to those in the mesons.

In order to show the dependence of quark SOC on the range of longitudinal momentum fraction x, we integrate C_z^q over $\mathbf{k}_\perp$ and show the variation of $C_z^q(x)$ with respect to x for various spin-0 mesons in Fig. 1. In Fig. 1(a), we present the most commonly studied mesons: the pion and the kaon. Here, it is observed that the largest contribution for the pion and kaon comes from the region where the longitudinal momentum fraction x is around 0.4 and 0.38, respectively. In Fig. 1(b), we present the η_b and η_c mesons and their highest x contribution comes at 0.5 and 0.5, respectively. The plots in this case are symmetric, which is due to a negligible difference in quark and antiquark masses. However, the C_z^q values for η_b and η_c are extremely low when compared to those of the pion and kaon. Similarly, in Fig. 1(c), we have considered the B mesons. The largest contribution for the B mesons B^+, B^0, B_s^0, and B_c^+ comes from regions where x is around 0.18, 0.18, 0.21, and 0.5, respectively. The peaks shift toward higher x values, which is due to the increasing inequality in the quark and antiquark masses inside the B mesons having the quark contents as $B^+(u\bar{b})$, $B^0(d\bar{b})$, $B_s^0(s\bar{b})$, and $B_c^+(c\bar{b})$. For the case where the quark is lighter than the other antiquark in the meson, a smaller longitudinal momentum fraction x is carried by the quark, hence, leading to the distribution peak at lower values of x. Further, in Fig. 1(d) the x dependence of $C_z^q(x))$ for all of the D mesons has been presented. The peak of the distribution for the D-mesons D^+, D^0, and D_s^+ has been observed at longitudinal momentum fractions of x equal to 0.7, 0.7, and 0.62, respectively. For D^+ and D^0, the quark (c) being heavier than the antiquark (u or d) carries a larger longitudinal momentum fraction x. This shifts the peak of the distribution to higher values of x, and the curve is shifted to the right. For the case of D_s^+, the difference between the quark (c) and the antiquark (s) is less compared to that of D^+ or D^0, and the distribution peaks at a comparatively lower x value.

Further, in Fig. 2 we have presented the dependence of the spin-orbit contribution with transverse momentum $\mathbf{k}_\perp$ at fixed values of longitudinal momentum fraction x. Figures 2(a), 2(c), and 2(e) show the dependence of SOC on the $\mathbf{k}_\perp$ using the GTMD approach, whereas Figs. 2(b), 2(d), and 2(f) show the dependence using the GPD approach. Figure 2(a) presents the variation of π^+, K^+, K^0, η_b, η_c at $x = 0.5$, Fig. 2(c) presents B^+, B^0, B_s^0, B_c^+ at $x = 0.7$, and Fig. 2(e) presents D^+, D^0, D_s^+ at $x = 0.3$. On the other hand, Fig. 2(b) presents the variation of

TABLE I. Model parameters for LFQM.

m_q	m_c	m_s	m_b	$\beta_{q\bar{q}}$	$\beta_{q\bar{c}}$	$\beta_{q\bar{b}}$	$\beta_{q\bar{s}}$	$\beta_{s\bar{c}}$	$\beta_{b\bar{b}}$	$\beta_{c\bar{c}}$	$\beta_{s\bar{b}}$	$\beta_{c\bar{b}}$
0.22	1.68	0.45	5.10	0.523	0.500	0.585	0.524	0.537	1.376	0.699	0.636	0.906

TABLE II. Spin-orbit correlation C_z^q for spin-0 mesons.

Spin-0 mesons	$C_z^{q/M}$
π^+	−0.272
K^+	−0.251
K^0	−0.251
B^+	−0.227
B^0	−0.227
B_s^0	−0.161
B_c^+	−0.035
D^+	−0.082
D^0	−0.082
D_s^+	−0.072
η_b	−0.031
η_c	−0.063

$\pi^+, K^+, K^0, \eta_b, \eta_c$ at $x = 0.4$, Fig. 2(d) presents B^+, B^0, B_s^0, B_c^+ at $x = 0.4$, and Fig. 2(f) presents D^+, D^0, D_s^+ at $x = 0.6$. It would be important to mention here that we have taken different values of x for each set to project the difference between different mesons. Keeping the same x values will not affect the dependence but will only affect the amplitude of the SOC. It is observed that even though we have the same C_z^q value for both the GTMD and GPD approaches, the transverse momentum dependence is different for them [50]. For the GTMD case, the $C_z^q(x, \mathbf{k}_\perp)$ is negative over the whole region of $\mathbf{k}_\perp$ for all the mesons, which is in agreement with the pion case detailed in Ref. [50]. We notice that for the mesons with light quarks, the peaks occur at lower values of $\mathbf{k}_\perp$ but with a comparatively large amplitude. The peaks are narrow and sharp for the light quark mesons, but as we increase the value of $\mathbf{k}_\perp$, they diminish and tend to zero. For the case of heavy quark mesons, the peaks appear at higher values of transverse momentum and are broader. The amplitudes also become quite small. Further, using the GPD approach, $C_z^q(x, \mathbf{k}_\perp)$ comes out to be positive for higher values of $\mathbf{k}_\perp$ in the case of π^+, K^+, K^0, η_b, η_c presented in Fig. 2(b) for $x = 0.4$. As the $\mathbf{k}_\perp$ values decrease, the $C_z^q(x, \mathbf{k}_\perp)$ value first decreases and then increases for the case of π^+. For η_c, it increases with decreasing $\mathbf{k}_\perp$, for K^+ and K^0, it decreases with decreasing $\mathbf{k}_\perp$, and for η_b there is a negligible increase in value with decreasing $\mathbf{k}_\perp$. These results are in agreement with the results in Ref. [50]. For the case of B mesons B^+, B^0, B_s^0, B_c^+ in Fig. 2(d), the variation of $C_z^q(x, \mathbf{k}_\perp)$ has been presented for $x = 0.4$. In these cases, the results are negative throughout the $\mathbf{k}_\perp$ region but tend to zero for higher values of $\mathbf{k}_\perp$. The SOCs for the D mesons presented in Fig. 2(f) for $x = 0.6$ remain positive but tend to zero beyond $\mathbf{k}_\perp = 1.00$ GeV. This opposite behavior of the

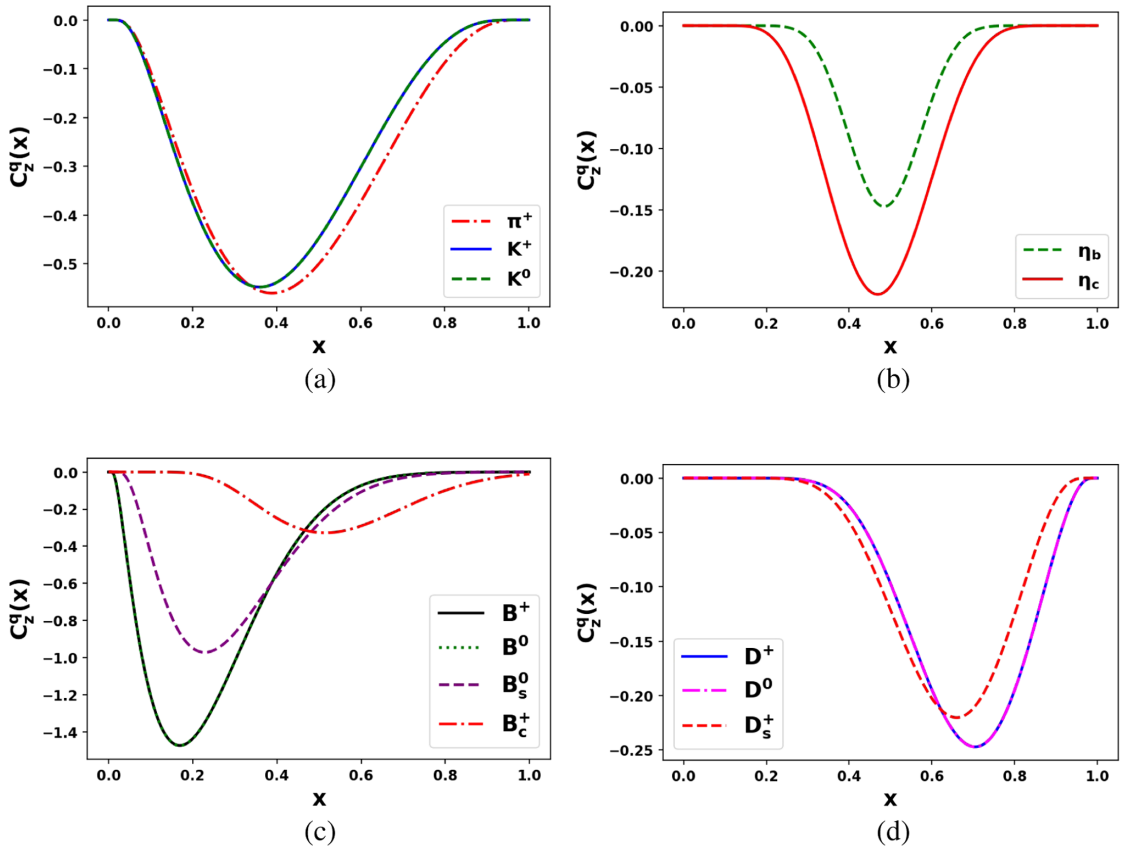

FIG. 1. x dependence of $C_z^q(x)$ for π^+, K^+ and K^0 (a), for η_b and η_c (b), for spin-0 B-mesons (c) and for spin-0 D-mesons (d).

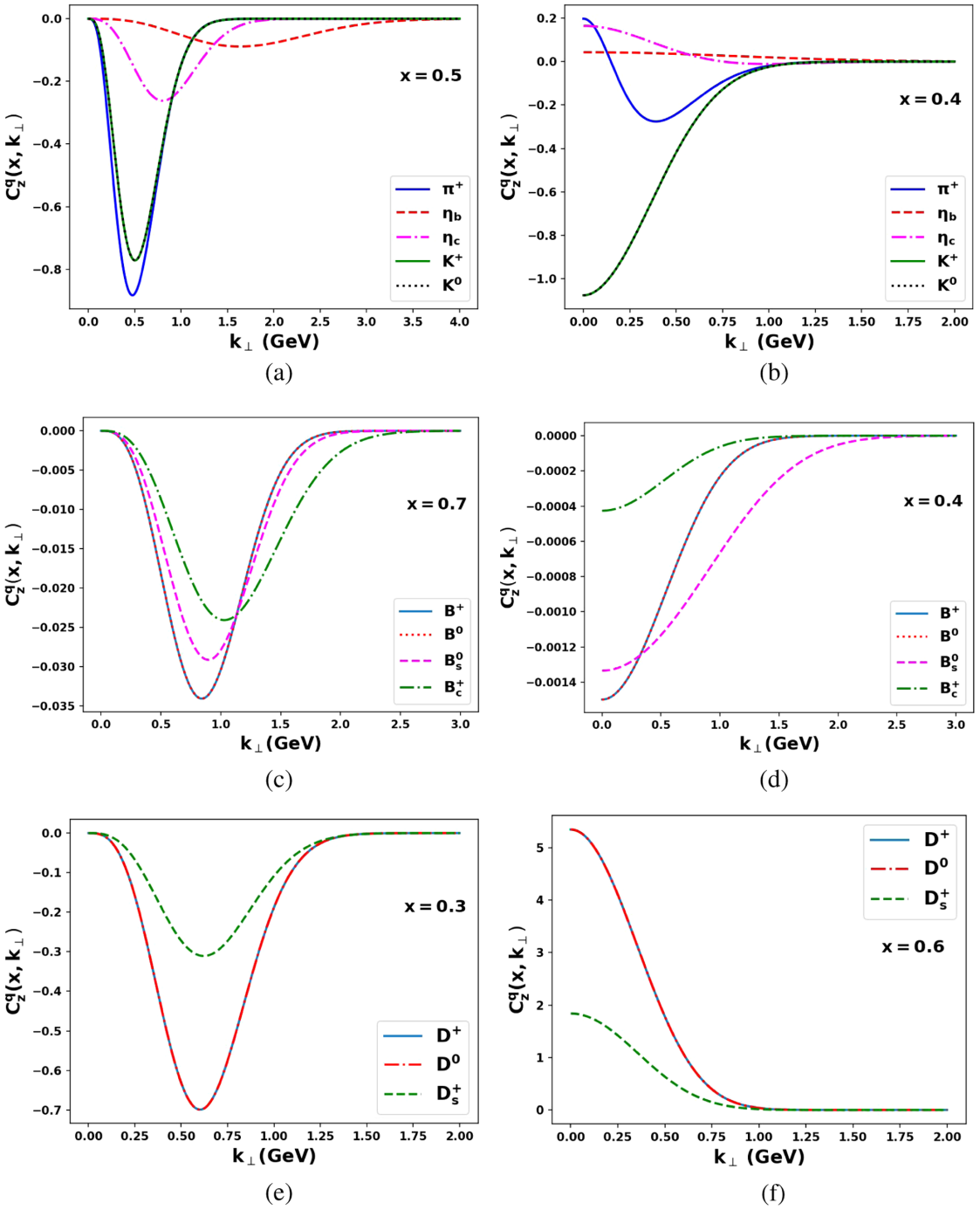

FIG. 2. $\mathbf{k}_\perp$ dependence of SOC $C_z^q(x, \mathbf{k}_\perp)$ at a fixed longitudinal momentum fraction x for spin-0 mesons. Panels (a), (c), and (e) show the dependence of SOC on the $\mathbf{k}_\perp$ using the GTMD approach, whereas panels (b), (d), and (f) show the dependence using the GPD approach.

B mesons and D mesons is due to the difference in the quark distributions having light and heavy masses, respectively.

We now compute the SOC for the case of spin-1 mesons. We consider Eq. (44) and replace the $G_{1,1}$ relation with the expression $g_1(x, \mathbf{k}_\perp)$ TMD from Eq. (64). The numerical results of C_z^q for the spectrum of spin-1 mesons having definite quark contents have been presented in Table III. The sign of the correlation comes out to be positive for spin-1 mesons implying that the quark OAM and the quark longitudinal spin tend to be directly aligned inside the respective spin-1 mesons. The difference between the alignment of SOC for the spin-1 meson and the spin-0 meson is because of the spin density term in the energy-momentum tensor defined in Eq. (35). There are only two

TABLE III. Spin-orbit correlation C_z^q for spin-1 mesons.

Spin-1 mesons	$C_z^{q/M}$
ρ^+	0.332
J/ψ	0.241
Υ	0.338
ϕ	0.221
K^{*+}	0.291
K^{*0}	0.291
B^{*0}	0.179
B^{*+}	0.179
B_s^{*0}	0.191
B_c^{*+}	0.224
D^{*0}	0.411
D^{*+}	0.411
D_s^{*+}	0.336

possibilities of the value of C_z^q, which can be either positive or negative depending on the alignment of the quark longitudinal spin and quark OAM. For the case of spin-1 mesons, positive values are obtained.

In Fig. 3, we have presented the dependence of C_z^q on longitudinal momentum fraction x for different spin-1 mesons. We discuss the cases of ρ^+, K^{*0}, and K^{*+} in Fig. 3(a) where the maximum contribution of $C_z^q(x)$ for ρ^+, K^{*0}, and K^{*+} is at 0.50, 0.48, and 0.48 respectively. In Fig. 3(b), we present the SOCs for J/ψ, ϕ, and Υ mesons. In this case, a symmetry is observed because of a similar quark content in the mesons. The largest contributions come approximately around 0.50 for all the mesons in this plot. In Fig. 3(c), we consider the B mesons, and the largest contribution for B^{*+}, B^{*0}, B_s^{*0}, and B_c^{*+} mesons is for the values of x at 0.10, 0.10, 0.12, and 0.30 for the respective mesons. Similar to the case of the spin-0 mesons, in the case on spin-1 mesons the quarks carry a smaller longitudinal momentum fraction x when the quark mass is lighter than its corresponding antiquark. This results in a peak at lower values of x, and the curve shifts toward the left. Finally, in Fig. 3(d), we present the D mesons. The highest x contribution for the D mesons D^+, D^0, and D_s^+ is found to be at $x = 0.22$, 0.22, and 0.28, respectively. The shifting of the peak is again due to the difference in the quark and antiquark masses giving a peak at higher values of longitudinal momentum fraction x when this difference is small.

In Fig. 4, we have shown the dependence of the spin-orbit contribution with transverse momentum $\mathbf{k}_\perp$ at fixed

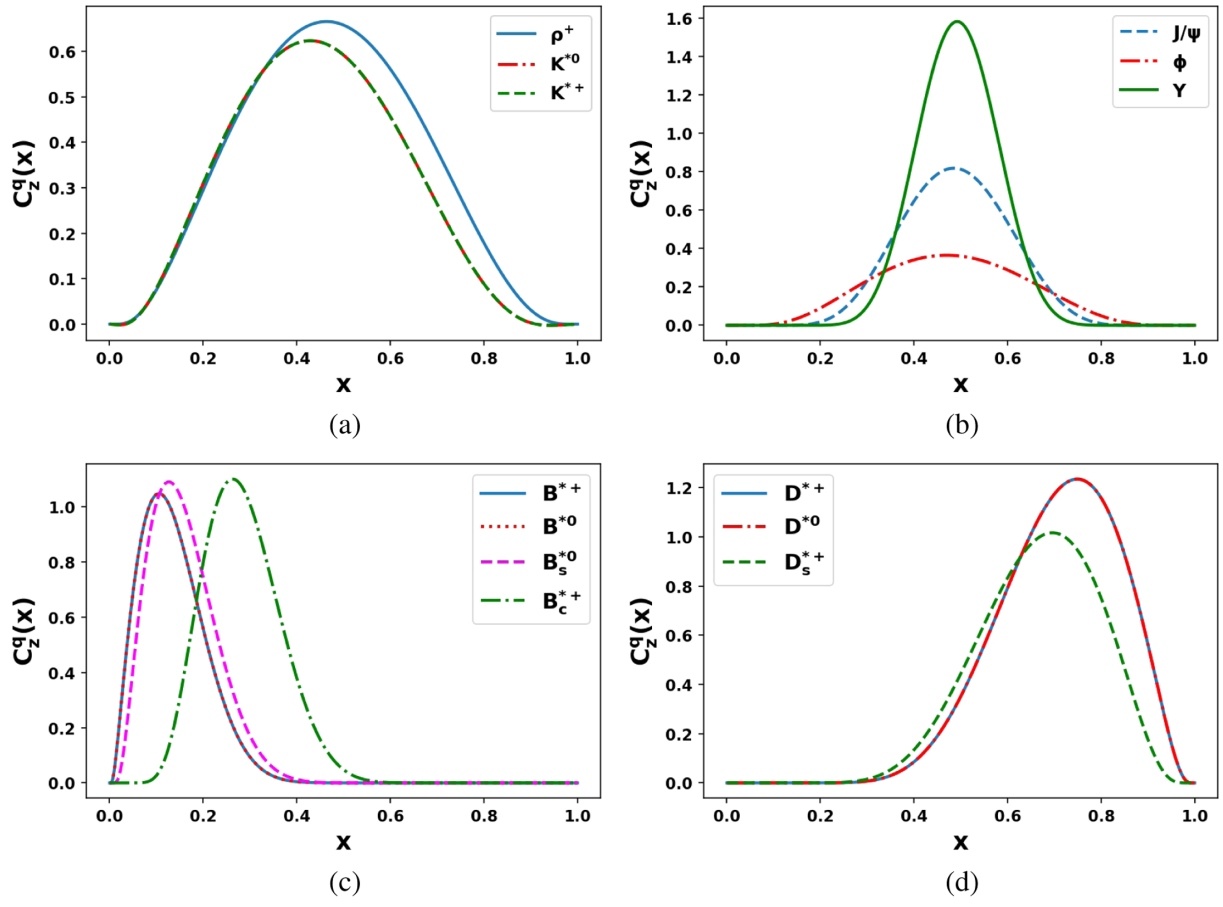

FIG. 3. x dependence of $C_z^q(x)$ for ρ^+, K^{*0} and K^{*+} (a), for J/Ψ, Φ and Υ (b), for spin-1 B-mesons (c) and for spin-1 D-mesons (d).

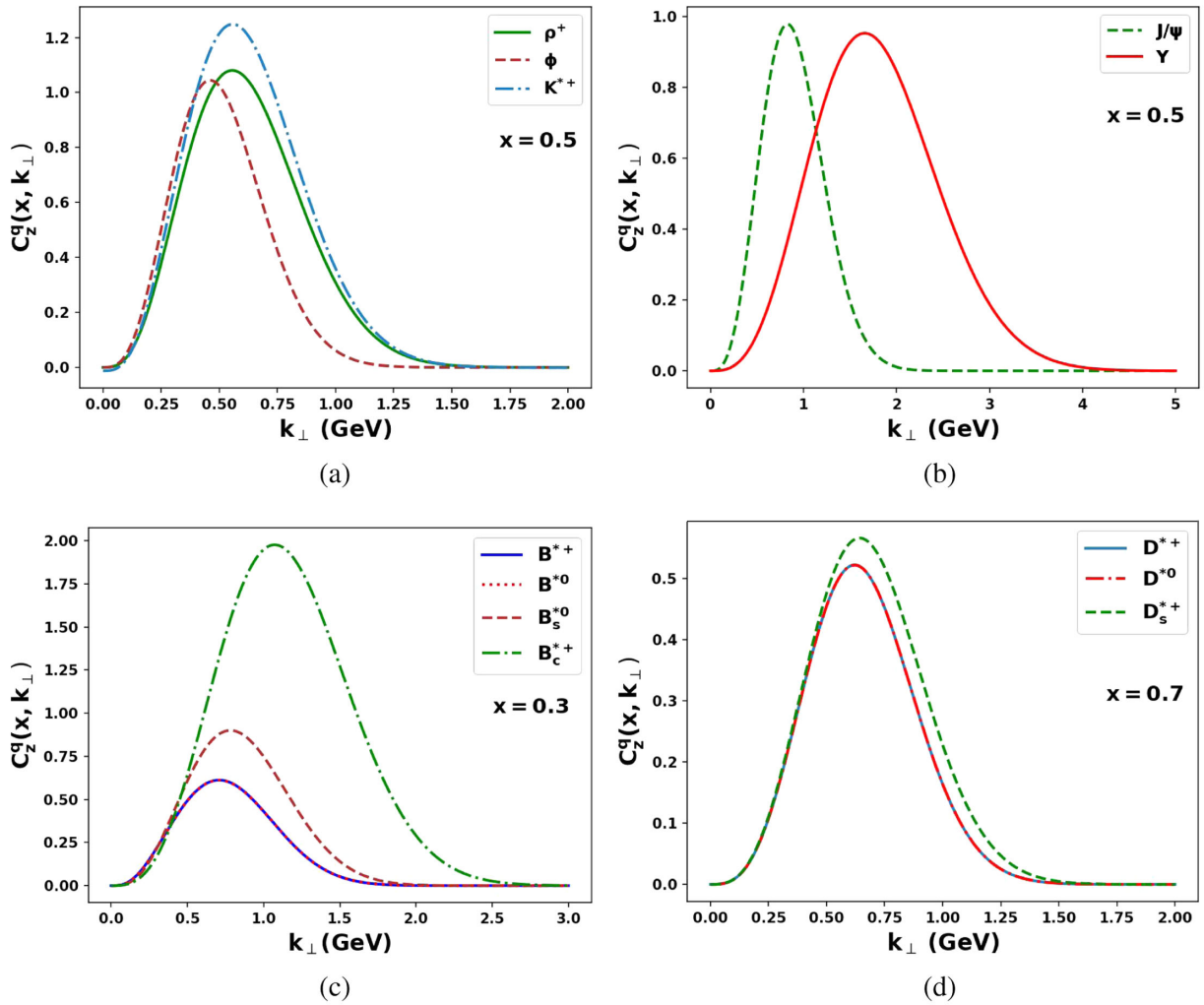

FIG. 4. $\mathbf{k}_\perp$ dependence of SOC $C_z^q(x, \mathbf{k}_\perp)$ at $x = 0.5$ for ρ^+, Φ and K^{*+} (a), at $x = 0.5$ for J/Ψ and Υ (b), at $x = 0.3$ for spin-1 B-mesons (c) and at $x = 0.7$ for spin-1 D-mesons (d) using GTMD approach.

values of longitudinal momentum fraction x for the spin-1 mesons using the GTMD approach. Figure 4(a) presents the variation of ρ^+, K^{*0}, and K^{*+} at $x = 0.5$, Fig. 4(b) presents J/ψ and Υ at $x = 0.5$, Fig. 4(c) presents B^{*+}, B^{*0}, B_s^{*0}, and B_c^{*+} at $x = 0.3$, and Fig. 4(d) presents D^+, D^0, and D_s^+ at $x = 0.7$. As discussed earlier, the peak of the quark distribution depends on the quark content of the meson. Mesons having similar quark and antiquark masses tend to have a higher amplitude for its distribution. For the case of mesons having a difference in the quark and antiquark masses, the amplitude varies in proportion to the mass difference. It is also observed that $C_z^q(x, \mathbf{k}_\perp)$ remains positive across the entire $\mathbf{k}_\perp$ region.

VI. SUMMARY AND CONCLUSION

In this work, we studied the correlation between the quark's orbital angular motion and the quark's longitudinal spin inside the light and heavy mesons with spin-0 and spin-1. We started by defining the gauge-invariant LF quark longitudinal OAM and decomposing it into its constituent left-handed and right-handed quark contributions. The quark SOC is described by the difference between the right- and left-handed quark contributions of this longitudinal OAM. We defined $\hat{T}^{\mu\nu}_{q5}$ and further decomposed it into two FFs out of which one form factor is the SOC ascertained by the form factor C_z^q. We considered two approaches in order to calculate C_z^q. One is the GTMD approach, where C_z^q is defined by the leading-twist correlator $G_{1,1}$ for the spin-0 mesons and $g_1(x, \mathbf{k}_\perp)$ for the case of spin-1 mesons. The alternative way is the GPD technique, in which the first x moments of $F_1^q(x, \zeta, t)$ and $H_1^q(x, \zeta, t)$ at $\zeta = 0$, $t = 0$ GeV^2 combine to yield the correlation's expectation value. We calculated the analytical results for C_z^q by considering the overlap representation of the GPDs and the GTMDs in LFQM. We listed the numerical results of C_z^q for both the spin-0 and spin-1

mesons. There is a small variation in our results on comparing them with the SOCs of the pion and kaon in the LFQM [50,66]. This variation is due to the different HO parameters and normalization constants. The negative sign in the case of spin-0 mesons indicates that the OAM and quark spin tend to be anticorrelated. The positive sign in the case of spin-1 mesons indicates that OAM and quark spin tend to be directly correlated. We presented the dependence of longitudinal momentum fraction x and the transverse momentum $\mathbf{k}_\perp$ for the longitudinal SOC where we considered $\mathbf{k}_\perp$ dependence for both the GPDs and GTMDs while dealing with spin-0 mesons and only the GTMDs in the context of spin-1 mesons. Since the spin-1 meson has an added spin wave part, we found that the dependence of longitudinal momentum fraction varies from the case of the spin-0 case. We presented fresh insights into the SOC inside the spin-0 and spin-1 mesons with our analysis of the quark longitudinal spin, which has not been investigated before except for the case of pions and kaons. This work helps us understand the spin structure of different mesons.

Future experimental data from SPD at the NICA collider at JINR (Dubna, Russia) [86,87] will provide deep insight into the spin structure of the hadrons. The upcoming new and upgraded experiments at JLab, DESY, EIC (electron-ion collider) [88] will in the future come up as a valuable sources in accessing the spin physics data, which will give extensive information to probe the multidimensional structure of hadrons.

ACKNOWLEDGMENTS

H. D. would like to thank the Science and Engineering Research Board, Anusandhan National Research Foundation, Government of India under the scheme SERB-POWER Fellowship (Reference No. SPF/2023/000116) for financial support.

[1] W. J. Marciano and H. Pagels, Phys. Rep. **36**, 137 (1978).
[2] A. J. Arifi, H. M. Choi, C. R. Ji, and Y. Oh, Phys. Rev. D **106**, 014009 (2022).
[3] G. Altarelli, Phys. Rep. **81**, 1 (1982).
[4] A. Bacchetta, F. Conti, and M. Radici, Phys. Rev. D **78**, 074010 (2008).
[5] C. Lorce and B. Pasquini, Phys. Rev. D **84**, 014015 (2011).
[6] Y. Han, T. Liu, and B.-Q. Ma, Phys. Lett. B **830**, 137127 (2022).
[7] R. Placakyte (H1 and ZEUS Collaborations), arXiv:1111.5452.
[8] A. D. Martin, R. G. Roberts, W. J. Stirling, and R. S. Thorne, Eur. Phys. J. C **4**, 463 (1998).
[9] M. Glück, E. Reya, and A. Vogt, Eur. Phys. J. C **5**, 461 (1998).
[10] M. Gluck, E. Reya, and A. Vogt, Z. Phys. C **67**, 433 (1995).
[11] P. J. Mulders and R. D. Tangerman, Nucl. Phys. **B461**, 197 (1996); **B484**, 538(E) (1997).
[12] S. Puhan and H. Dahiya, Phys. Rev. D **109**, 034005 (2024).
[13] R. Angeles-Martinez *et al.*, Acta Phys. Pol. B **46**, 2501 (2015).
[14] D. Boer and P. J. Mulders, Phys. Rev. D **57**, 5780 (1998).
[15] D. Boer, Phys. Rev. D **60**, 014012 (1999).
[16] J. P. Ralston and D. E. Soper, Nucl. Phys. **B152**, 109 (1979).
[17] A. Kotzinian, Nucl. Phys. **B441**, 234 (1995).
[18] M. Radici, J. Phys. Conf. Ser. **527**, 012025 (2014).
[19] D. W. Sivers, Phys. Rev. D **41**, 83 (1990).
[20] M. Garcon, Eur. Phys. J. A **18**, 389 (2003).
[21] A. V. Belitsky and A. V. Radyushkin, Phys. Rep. **418**, 1 (2005).
[22] M. Diehl, Eur. Phys. J. A **52**, 149 (2016).
[23] D. Chakrabarti and A. Mukherjee, Phys. Rev. D **72**, 034013 (2005).
[24] S. J. Brodsky, D. Chakrabarti, A. Harindranath, A. Mukherjee, and J. P. Vary, Phys. Rev. D **75**, 014003 (2007).
[25] A. Rajan, A. Courtoy, M. Engelhardt, and S. Liuti, Phys. Rev. D **94**, 034041 (2016).
[26] P. Hagler, A. Mukherjee, and A. Schafer, Phys. Lett. B **582**, 55 (2004).
[27] X. Ji, Annu. Rev. Nucl. Part. Sci. **54**, 413 (2004).
[28] D. Chakrabarti, T. Maji, C. Mondal, and A. Mukherjee, Eur. Phys. J. C **76**, 409 (2016).
[29] A. Bacchetta, F. Delcarro, C. Pisano, M. Radici, and A. Signori, J. High Energy Phys. 06 (2017) 081; 06 (2019) 51.
[30] S. J. Brodsky, H. C. Pauli, and S. S. Pinsky, Phys. Rep. **301**, 299 (1998).
[31] J. C. Collins, Phys. Lett. B **536**, 43 (2002).
[32] J. Zhou, F. Yuan, and Z. T. Liang, Phys. Rev. D **81**, 054008 (2010).
[33] R. D. Tangerman and P. J. Mulders, Phys. Rev. D **51**, 3357 (1995).
[34] J. T. Donohue and S. A. Gottlieb, Phys. Rev. D **23**, 2577 (1981).
[35] S. Catani, D. de Florian, G. Ferrera, and M. Grazzini, J. High Energy Phys. 12 (2015) 047.
[36] I. Scimemi and A. Vladimirov, Eur. Phys. J. C **78**, 89 (2018).
[37] J. C. Collins, D. E. Soper, and G. F. Sterman, Nucl. Phys. **B250**, 199 (1985).
[38] D. Müller, D. Robaschik, B. Geyer, F. M. Dittes, and J. Hořejři, Fortschr. Phys. **42**, 101 (1994).
[39] S. Boffi and B. Pasquini, Riv. Nuovo Cimento **30**, 387 (2007).
[40] K. Goeke, M. V. Polyakov, and M. Vanderhaeghen, Prog. Part. Nucl. Phys. **47**, 401 (2001).
[41] A. V. Radyushkin, Phys. Lett. B **380**, 417 (1996).

[42] L. Mankiewicz, G. Piller, and T. Weigl, Eur. Phys. J. C **5**, 119 (1998).
[43] L. L. Frankfurt, P. V. Pobylitsa, M. V. Polyakov, and M. Strikman, Phys. Rev. D **60**, 014010 (1999).
[44] C. Lorcé and B. Pasquini, J. High Energy Phys. 09 (2013) 138.
[45] S. Meissner, A. Metz, and M. Schlegel, J. High Energy Phys. 08 (2009) 056.
[46] X. D. Ji, Phys. Rev. Lett. **78**, 610 (1997).
[47] E. Leader and C. Lorcé, Phys. Rep. **541**, 163 (2014).
[48] S. Kaur, N. Kumar, J. Lan, C. Mondal, and H. Dahiya, Phys. Rev. D **102**, 014021 (2020).
[49] R. L. Jaffe and A. Manohar, Nucl. Phys. **B337**, 509 (1990).
[50] C. Tan and Z. Lu, Phys. Rev. D **105**, 034004 (2022).
[51] A. Harindranath, arXiv:hep-ph/9612244.
[52] M. V. Terentev, Sov. J. Nucl. Phys. **24**, 106 (1976).
[53] A. J. Arifi, H. M. Choi, C. R. Ji, and Y. Oh, Phys. Rev. D **107**, 053003 (2023).
[54] G. P. Lepage and S. J. Brodsky, Phys. Rev. D **22**, 2157 (1980).
[55] T. Jacobson, Lect. Notes Phys. **870**, 1 (2013).
[56] W. Jaus, Phys. Rev. D **41**, 3394 (1990).
[57] W. Jaus, Phys. Rev. D **44**, 2851 (1991).
[58] F. Coester and W. N. Polyzou, Phys. Rev. C **71**, 028202 (2005).
[59] V. M. Belyaev and M. B. Johnson, Phys. Lett. B **423**, 379 (1998).
[60] A. J. Arifi, P. T. P. Hutauruk, and K. Tsushima, Phys. Rev. D **107**, 114010 (2023).
[61] J. P. B. C. de Melo, T. Frederico, E. Pace, and G. Salme, Phys. Lett. B **581**, 75 (2004).
[62] J. P. B. C. de Melo and T. Frederico, Phys. Rev. C **55**, 2043 (1997).
[63] H. M. Choi, Phys. Rev. D **103**, 073004 (2021).
[64] H. J. Melosh, Phys. Rev. D **9**, 1095 (1974).
[65] C. Lorcé, Phys. Lett. B **735**, 344 (2014).
[66] S. Kaur and H. Dahiya, Phys. Rev. D **100**, 074008 (2019).
[67] K. Tanaka, Phys. Rev. D **98**, 034009 (2018).
[68] M. V. Polyakov and P. Schweitzer, Int. J. Mod. Phys. A **33**, 1830025 (2018).
[69] A. F. Krutov and V. E. Troitsky, Phys. Rev. D **103**, 014029 (2021).
[70] A. Freese and I. C. Cloët, Phys. Rev. C **100**, 015201 (2019); **105**, 059901(E) (2022).
[71] Z. L. Ma and Z. Lu, Phys. Rev. D **98**, 054024 (2018).
[72] S. J. Brodsky, T. Huang, and G. P. Lepage, Springer Tracts Mod. Phys. **100**, 81 (1982).
[73] P. Hoyer, Int. J. Mod. Phys. A **04**, 4535 (1989).
[74] J. h. Yu, B. W. Xiao, and B. Q. Ma, J. Phys. G **34**, 1845 (2007).
[75] W. Qian and B. Q. Ma, Phys. Rev. D **78**, 074002 (2008).
[76] M. Diehl, Phys. Rep. **388**, 41 (2003).
[77] B. Q. Ma, Z. Phys. C **58**, 479 (1993).
[78] T. Liu and B. Q. Ma, Phys. Rev. D **91**, 034019 (2015).
[79] S. Puhan, S. Sharma, N. Kaur, N. Kumar, and H. Dahiya, J. High Energy Phys. 02 (2024) 075.
[80] S. Kaur, C. Mondal, and H. Dahiya, J. High Energy Phys. 01 (2021) 136.
[81] B. W. Xiao, X. Qian, and B. Q. Ma, Eur. Phys. J. A **15**, 523 (2002).
[82] M. Burkardt and B. Hannafious, Phys. Lett. B **658**, 130 (2008).
[83] A. Metz, S. Meissner, and M. Schlegel, Mod. Phys. Lett. A **24**, 2973 (2009).
[84] M. G. Echevarria, A. Idilbi, K. Kanazawa, C. Lorcé, A. Metz, B. Pasquini, and M. Schlegel, Phys. Lett. B **759**, 336 (2016).
[85] M. Diehl, T. Feldmann, R. Jakob, and P. Kroll, Nucl. Phys. **B596**, 33 (2001); **B605**, 647(E) (2001).
[86] A. Guskov (SPD Working Group), J. Phys. Soc. Jpn. Conf. Proc. **26**, 021018 (2019).
[87] O. Kouznetsov and I. Savin, Nucl. Part. Phys. Proc. **282–284**, 20 (2017).
[88] R. Abdul Khalek *et al.*, Nucl. Phys. **A1026**, 122447 (2022).